Fatigue Behavior of Y–Ba–Cu–O/Hastelloy-C Coated Conductor at 77 K

Abdallah L. Mbaruku and Justin Schwartz, *Fellow, IEEE*

***Abstract*—Superconducting materials are subjected to various loading in motors, transformers, generators, and other magnet applications. The loading conditions include bending, tension, compression, and fatigue, and result from coil manufacturing, thermal cycling, quenching, and normal operation. Each of these loading conditions can affect the performance of the superconductor and thus the magnet and system. It is important, therefore, to understand the electromechanical behavior of the superconducting material to optimize the design. Here we report the effects of mechanical fatigue at 77 K on the electrical transport properties of $YBa_2Cu_3O_{7-\delta}$/Hastelloy-C coated conductors. The effects of longitudinal tensile fatigue on the critical current and the n-value are reported. Strain controlled fatigue studies include strains up to 0.495% and strain ratios of 0.2 and 0.5. Scanning electron micrographs of the fatigued conductors are used to identify the sources of failure. Crack formation is believed to be the cause of I_c degradation in fatigued samples. Further, the fatigue strength and ductility behaviors analyzed using a 5% reduction in I_c as the electrical definition of failure showed that the fatigue strength exponent is within the values found for metals but both the fatigue ductility coefficient and exponent show that the material tested is brittle.**

***Index Terms*—Coated conductors, electromechanical properties, fatigue effects, Y–Ba–Cu–O.**

I. Introduction

DURING application, high-temperature superconducting (HTS) materials are subjected to various stresses that include bending, tension, compression, and fatigue. At least four possible sources of fatigue stresses in superconductors are known. First, repeated thermal cycling causes prestressing in the superconductor to occur in a cyclic (fatigue) mode. This occurs in between applications due to repetitive cool-down and removal from the cryogen or low temperature when not in use or due to quenching of the coil. The second source involves applications that use alternating current, in which any stress due to the Lorentz force will vary periodically at the same frequency as the current, causing fatigue stresses. Rotational (centrifugal) stress is the third source and occurs in applications involving rotating machines like motors and generators. This type of stress occurs mostly during starting from rest and vice versa, and when the load is varied. Lastly, there can be random loads in mobile systems and in particular in proposed airborne systems [1]. These load cycles are less predictable and thus require design margin.

Fatigue behavior of HTS materials has been studied by several research teams, especially in the wake of good progress in wire/tape manufacturing, their costs, and improvement in cooling devices during application. Kitaguchi *et al.* [2] observed no I_c degradation between strains of -0.2% and 0.2% and up to 5000 fatigue cycles on $Bi_2Sr_2Ca_2Cu_3O_y$ (Bi2223) tapes at 77 K. However, there was a steep decrease in the I_c with increasing number of cycles for a strain of 0.33%. Sugano *et al.* [3] did similar work and identified the cause of degradation of I_c as fracture of the Bi2223 filaments.

Malachevsky and Esparza [4] performed bending fatigue tests on Bi2223 tapes and observed that for high bending strain, the I_c of monofilamentary tape degraded after a few cycles compared to 7 and 19 filaments tapes. Holtz and Gubser [5] observed that room temperature longitudinal fatigue strength at 10^7 cycles for Bi2223 reinforced tape is comparable to its yield stress, while at 77 K the fatigue strength is the same as that for mechanical failure. Holtz *et al.* [6] also showed that the maximum fatigue tolerant c-axis tensile stress to 10^5 cycles was about 24 MPa for the reinforced Bi2223 tape conductor.

Salazar *et al.* [7] studied fatigue behavior of three different multifilamentary Ag/Bi2223 superconducting tapes and concluded that there is an increased strength of the tapes when the sheath is alloyed with Mg or when the tape is reinforced with steel foils. Shin studied fatigue behavior of Ag alloyed Bi2223 [8], [9] and steel foil reinforced [10] Bi2223 superconducting tapes at two different stress ratios, and showed that steel reinforced tapes have higher fatigue limits than Mn-sheath alloyed tapes. An increase in electrical and mechanical fatigue limits was observed when the stress ratio was increased from 0.1 to 0.5 for both tapes.

Ekin *et al.* [11] studied transverse fatigue effects on I_c in $YBa_2Cu_3O_{7-\delta}$ (YBCO) coated ion beam assisted deposition (IBAD) tapes and showed that there is an additional 2% degradation in J_c from the static loading that was subjected to the tape prior to fatigue testing to 2000 cycles with 122-MPa stress amplitude. Improvement of transverse stress tolerance for magnet applications was recommended. Cheggour *et al.* [12] studied cyclic transverse stress tests on nickel and nickel-alloy RABiTS samples that were previously subjected to monotonic stresses. They showed that fatigue cycles do not create new cracks on samples that previously did not have their J_c degraded. However, fatigue cycles further degraded the J_c on samples that had J_c degraded from the previous monotonic loading. Cheggour *et*

Manuscript received October 4, 2007; revised April 16, 2008. Current version published September 4, 2008. This work was supported by the U.S. Department of Energy through the Center for Advanced Power Systems (CAPS) and the U.S. Air Force Office for Scientific Research. This paper was recommended by Associate Editor J. O. Willis.

A. L. Mbaruku is with the Department of Engineering Materials, College of Engineering and Technology, University of Dar es Salaam, Dar es Salaam, Tanzania (e-mail: mbaruku@udsm.ac.tz; mbaruku@magnet.fsu.edu).

J. Schwartz is with the Department of Mechanical Engineering and National High Magnetic Field Laboratory, Florida State University, Tallahassee, FL 32310 USA (e-mail: schwartz@magnet.fsu.edu).

Color versions of one or more of the figures in this paper are available online at http://ieeexplore.ieee.org.

Digital Object Identifier 10.1109/TASC.2008.2003491

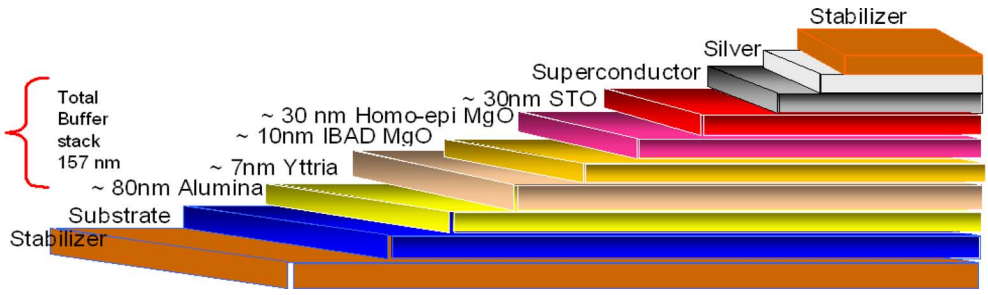

Fig. 1. Architecture of YBCO conductor used for fatigue test. The thicknesses of the different layers are shown.

al. [13] also studied effects of transverse compressive fatigue stress on slit Y–Ba–Cu–O coated conductors in which samples were subjected to up to 20 000 cycles. It was found that under the testing conditions, the damage on the edges of the conductor from slitting process does not worsen. They cautioned, however, that slitting may still potentially weaken the conductor performance in other loading cases.

Most research has focused on fatigue behavior of Bi2223 tapes and only a few have studied fatigue behavior for the YBCO coated conductor, though the YBCO coated conductor is now available in lengths greater than 100 m [14], . Thus, there is a need to investigate fatigue behavior of the YBCO conductor so that an engineering database can be developed, and to better understand the failure mechanism in these conductors.

II. Experiments

A. Samples and Their Preparation

All samples were from the same batch of YBCO coated conductor from SuperPower Inc. YBCO films were grown on IBAD-MgO and on 50-μm-thick Hastelloy-C substrates on a 1.2-cm width, and then slit into 4-mm-wide tapes. The slit tapes were then plated with copper ($\sim$20 μm thick) all around (40 μm total). Each sample was 55 mm long, 4.1 mm wide, and 0.1 mm thick. Fig. 1 shows a detailed architecture of the conductor used in this work.

To observe the microstructures of the YBCO coated conductors in the environmental scanning electron microscope (ESEM) before and after fatigue testing, etching of the Cu layer on the YBCO side was performed using a diluted nitric acid (30%vol. HNO_3: 70%vol. H_2O) followed by that of silver using a solution of 25%vol. H_2O_2: 25%vol. NH_4OH: 50%vol. H_2O that was freshly made every time. The samples were rinsed with water to remove the nitric acid before starting the silver etching process. Prior to the etching process, a thin layer of nail varnish was applied on all sample edges and other surfaces to prevent etching undesired areas.

B. Testing

Prior to fatigue testing, strain-I_c measurements were made to determine the maximum strain before I_c degradation in single-cycle mode. Longitudinal fatigue testing was performed in tension–tension strain-controlled mode, whereby the strain limits were fixed for a given sample but varied from one sample to another. Samples were fatigued using a tension–tension strain controlled fatigue mode up to a to 2×10^5 cycles with strain ratios (R) of 0.2 and 0.5 at a frequency of 0.4 Hz. This is the maximum frequency for equipment stability. All testing was done at 77 K in liquid nitrogen. The maximum strains were 0.350%, 0.400%, 0.450%, and 0.495% for $R = 0.2$ and 0.350%, 0.367%, 0.380%, and 0.400% for $R = 0.5$. Both the strain-I_c and fatigue-I_c tests were performed using a low-temperature electromechanical testing device described in detail in [15] and [16]. I_c was measured after cycles 1, 10, 100, 1000, and every 5000 thereafter until either $I_c < 4$ A or 2×10^5 fatigue cycles (N) have been reached. $N = 2 \times 10^5$ is a system limit above which the gears on the testing device require replacement. All I_c measurements were performed using the four-point method at self-field and a 1-μV/cm criterion. The conductor *n-value* is also obtained during I_c measurement, where the $V(I)$ data is fitted using $V \sim I^n$, thus quantifying the sharpness of the transition [17]. The electric field range in which *n-value* is determined is 0 to 10 μV/cm.

III. Results

Strain-I_c and stress–strain results shown in Fig. 2 show that the onset of I_c degradation occurs at $\varepsilon \sim 0.59\%$ which was taken to be the upper limit in the fatigue tests. Fig. 3 shows the result of fatigue tests for a strain ratio of 0.5 where normalized $I_c(I_c(N)/I_c(N=0))$ versus N is plotted on a log scale. No I_c degradation occurred for samples tested with a maximum strain of 0.350% and 0.367%, while there is gradual I_c degradation for samples tested at 0.380% and 0.400% maximum strains.

Fig. 4 shows the result for *n-value* versus N on a log scale for the fatigue tests performed with $R = 0.5$, corresponding to the data in Fig. 3. Samples subjected to 0.350% and 0.367% maximum strain have their respective *n-values* after fatigue testing relatively unchanged, while *n-values* for 0.380% and 0.400% have a decreasing trend that follows the I_c degradation.

Fig. 5. $I_c(N)/I_c(N=0)$ versus N on a log scale for $R = 0.2$. I_c did not degrade for a sample tested with 0.350% maximum strain, while degradation is observed for all other samples. Fig. 6 shows the corresponding *n-value* versus N for the same fatigue tests. As with I_c, samples subjected to 0.350% maximum strain showed no change and all other samples show degradation with increasing N.

Fig. 7 shows an SEM micrograph of a fatigued sample that showed a 53% reduction in I_c ($R = 0.5$, $N = 2 \times 10^5$, $\varepsilon_{\max} = 0.400\%$). Cracks are clearly seen but are not widespread in the sample; rather they are localized starting from the edge. As one

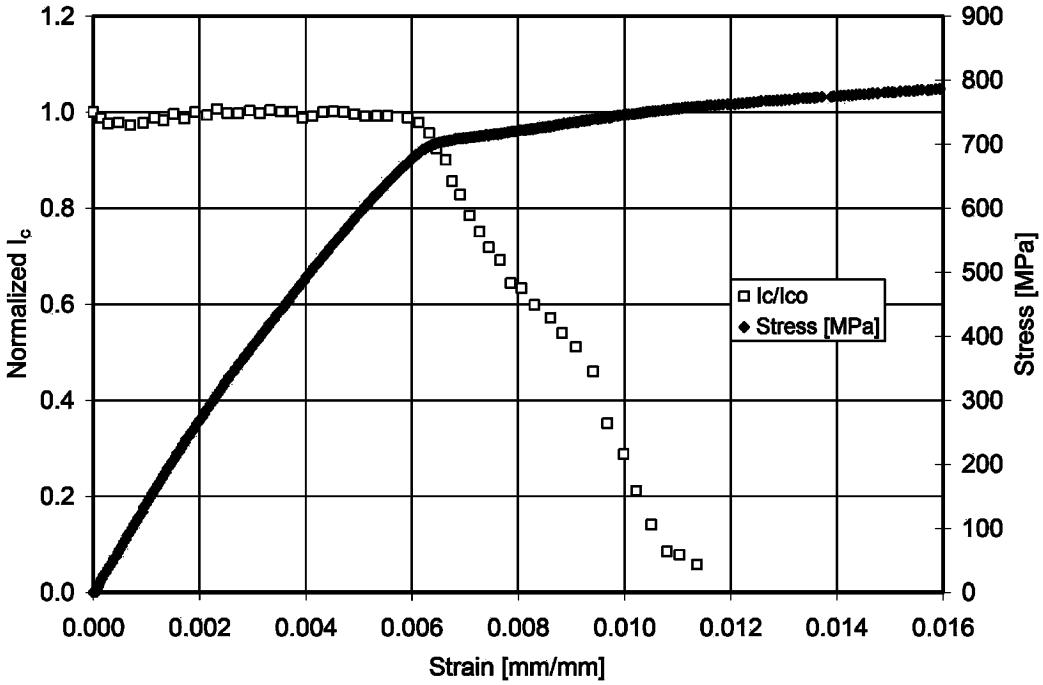

Fig. 2. $I_c(\varepsilon)/I_c(\varepsilon = 0)$ versus ε. Test performed at 77 K, using the four-point method at self field and a 1-μV/cm criterion. $I_c(\varepsilon = 0) = 60.77$ A. Also shown is the corresponding σ-ε data. Young's modulus is 140 GPa and yield stress based on 0.2% offset is 740 MPa.

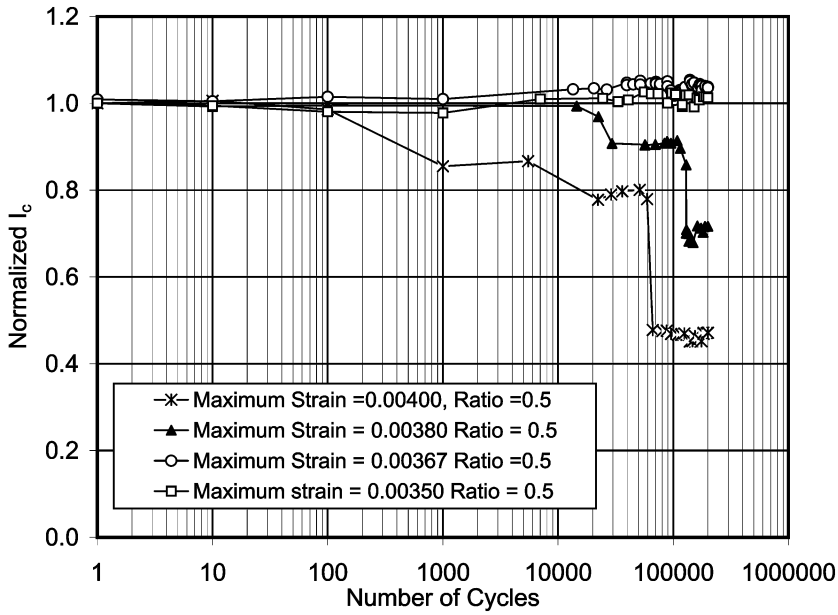

Fig. 3. $I_c(N)/I_c(N = 0)$ versus N for samples subjected to fatigue test with a strain ratio of 0.5. No current degradation for samples subjected 0.350% and 0.367% is observed.

moves from the edge (right side of the figure) to the center of the conductor (left side of the figure), the size and number of cracks clearly decreases. Fig. 8(a) shows an ESEM image of a cracked area of a fatigued sample with I_c degraded completely ($R = 0.2$, $N = 1.59 \times 10^5$, $\varepsilon_{\max} = 0.400\%$), and Fig. 8(b) is an ESEM image for a fatigued sample with no reduction in I_c ($R = 0.5$, $N = 2 \times 10^5$, $\varepsilon_{\max} = 0.350\%$). Some of the cracks seen in Fig. 8(a) are larger than those seen in Fig. 7; no cracks are observed in Fig. 8(b). Thus, the images in Figs. 7 and 8 show a clear correlation between crack growth and reductions in I_c during fatigue.

IV. Analysis

Consider the illustration of a fully reversed stress–strain loop shown in Fig. 9. The total true strain range in a fatigue test can be represented as

$$\Delta\varepsilon = \Delta\varepsilon_p + \Delta\varepsilon_e \tag{1}$$

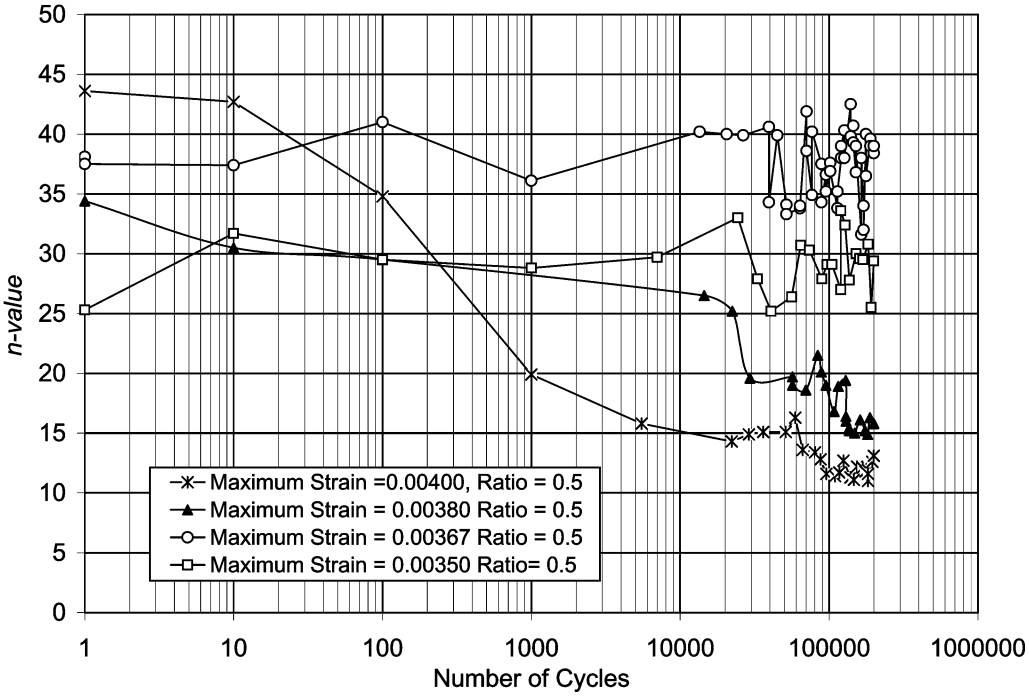

Fig. 4. *n-value* versus N for fatigued samples with $R = 0.5$.

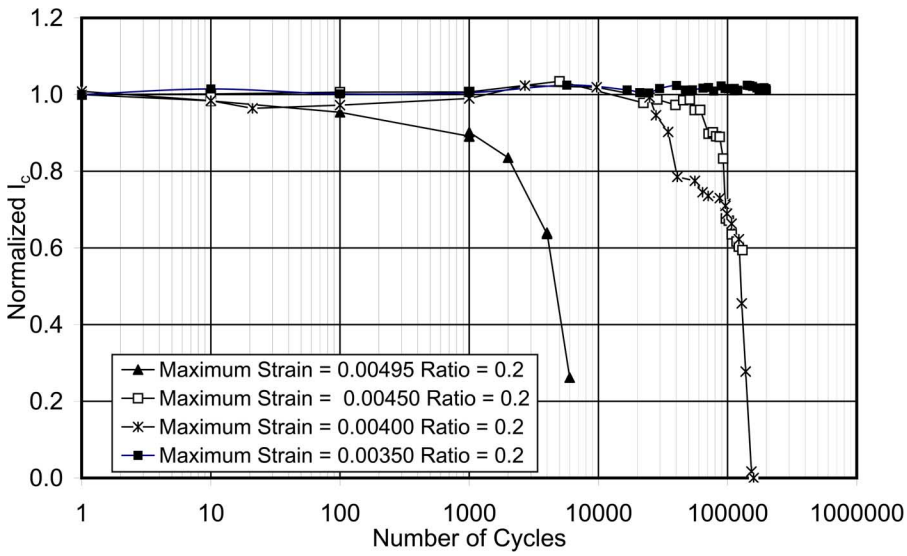

Fig. 5. $I_c(N)/I_c(N = 0)$ versus N for fatigue testing with $R = 0.2$. With the exception of the sample with maximum strain of 0.350%, I_c degrades with increasing N.

where $\Delta\varepsilon$ is the total true strain range, $\Delta\varepsilon_p$ is the true plastic strain range, and $\Delta\varepsilon_e$ is the true elastic strain range. But for the loop, the total true strain range is equal to twice the true strain amplitude, i.e.,

$$\Delta\varepsilon = 2\Delta\varepsilon_a. \tag{2}$$

The total true stress range is equal to twice the true stress amplitude, i.e.,

$$\Delta\sigma = 2\sigma_a. \tag{3}$$

Basquin [18] showed that a log-log plot of true stress amplitude versus number of reversals produces a linear relationship given by

$$\sigma_a = \frac{\Delta\sigma}{2} = \sigma'_f(2N_f)^b \tag{4}$$

where $\Delta\sigma/2(= \sigma_a)$ is the true stress amplitude, $2N_f$ is the number of reversals to failure, σ'_f is the fatigue strength coefficient, and b is fatigue strength exponent. σ'_f and b are fatigue properties of the material.

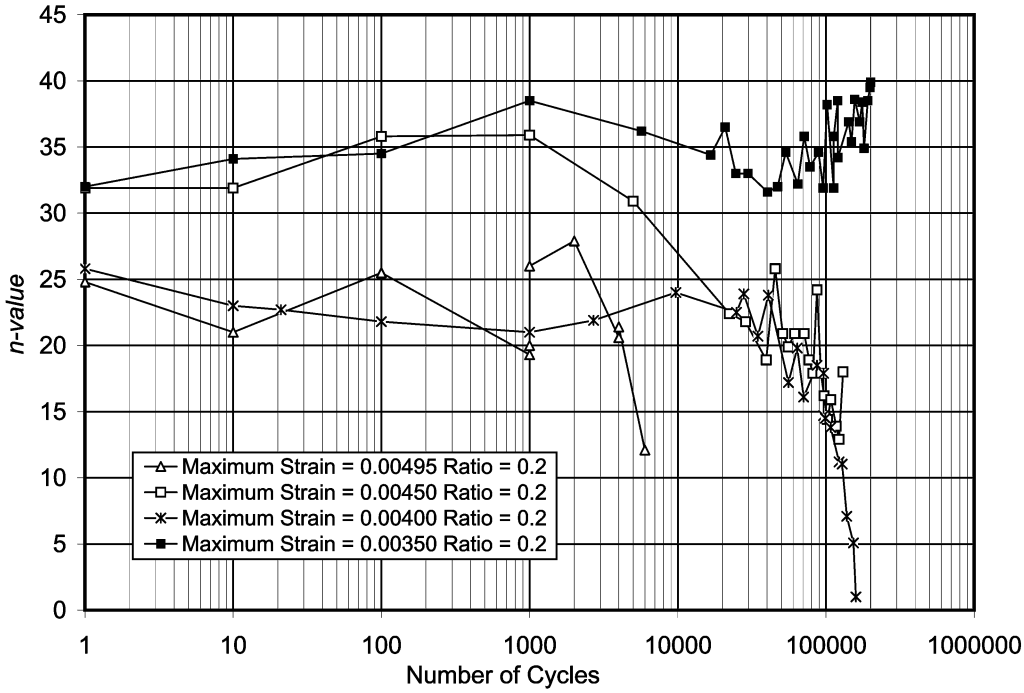

Fig. 6. *n-value* versus N results for fatigued samples with $R = 0.2$. With the exception of the sample with 0.350% maximum strain, the *n-values* decrease with increasing N.

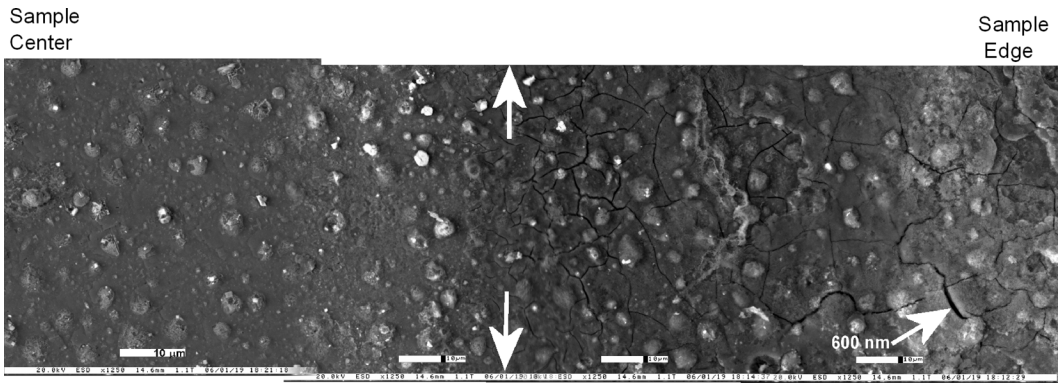

Fig. 7. Typical scanning electrcon micrograph of a fatigued sample with a 53% reduction in I_c. In this case, $R = 0.5$, $N = 2 \times 10^5$ and $\varepsilon_{\max} = 0.400\%$. The right side of the image is near the sample edge while the left side is near the sample center. The vertical arrows indicate the direction of both current flow during I_c measurement and applied load during fatigue. The crack indicated with an arrow has a width of ~600 nm. Note that the far left side of the image shows no cracks and overall ~50% of the sample shows a crack network, consistent with the I_c reductrion measured. The sample width seen on the image is ~1.5 mm, which is ~75% of the conductor half-width.

Coffin [19] and Manson [20] found that the true plastic strain amplitude data could also be linearized on a log-log scale as given

$$\frac{\Delta\varepsilon_p}{2} = \varepsilon'_f(2N_f)^c \tag{5}$$

where $\Delta\varepsilon_p/2$ is the true plastic strain amplitude, $2N_f$ is the number of reversals to failure, ε'_f is the fatigue ductility coefficient, and c is fatigue ductility exponent. ε'_f and c are also fatigue properties of the material.

A modified definition of the number of reversals to failure $(2N_f)$ in (4) and (5) is made to reflect the use of superconducting materials. Superconductivity failure is defined electrically rather than mechanically. Therefore, the number of reversals to failure is defined in this case as the number of reversals that cause the I_c to degrade to 95% of its initial value. The data obtained from the fatigue tests is modified to obtain true stresses and strains at 95% performance. The values of σ'_f and ε'_f are obtained from data such that $I_c(\varepsilon) = 0.95I_c(\varepsilon = 0)$.

The data obtained from the fatigue tests are modified to obtain true stresses and strains based upon the 95% performance criterion described above using

$$\varepsilon_t = \ln(1+\varepsilon) \tag{6}$$

and

$$\sigma_t = \sigma(1+\varepsilon) \tag{7}$$

where ε_t is the true strain, ε is the engineering strain, σ_t is the true stress, and σ is the engineering stress.

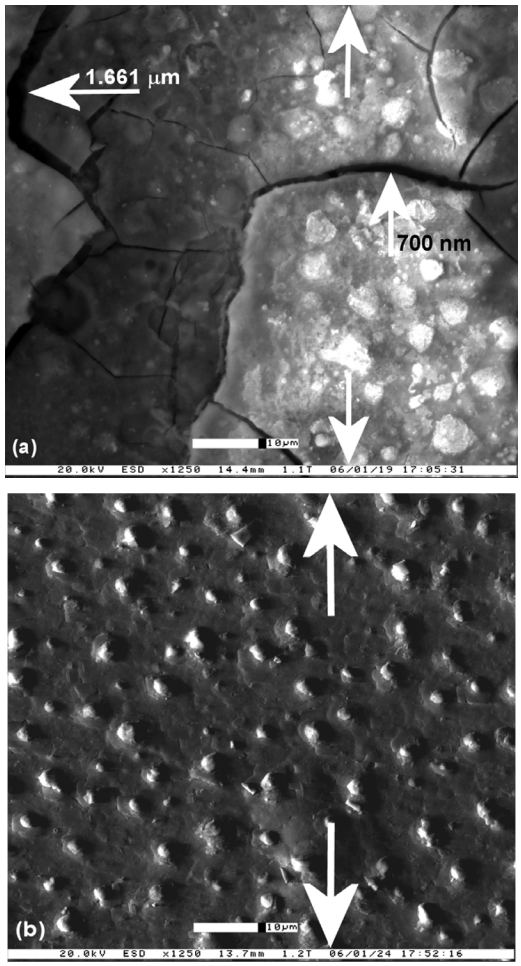

Fig. 8. Scanning electrcon micrographs of fatigued samples with I_c (a) degraded completely before reaching 2×10^5 cycles ($R = 0.2$, $N = 159\,000$, $\varepsilon_{\max} = 0.400\%$) and (b) fatigued to the maximum number of cycles allowed by the system (2×10^5) without any I_c degradation ($R = 0.5, \varepsilon_{\max} = 0.350\%$). The vertical arrows at the top and bottom of the images represent the loading direction. Note that some cracks in (a) are larger than those in Fig. 7 and that no cracks are seen in (b). These images are typical of the entire widths of these samples.

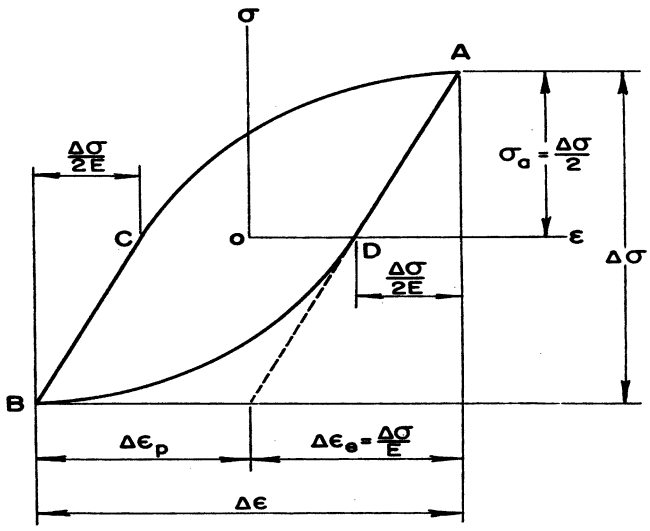

Fig. 9. Illustration of stress–strain hysteresis loop in fully reversed loading.

The true plastic strain amplitudes are calculated from

$$\varepsilon_{\mathrm{pa}} = \varepsilon_{\mathrm{ta}} - \frac{\sigma_a}{E} \tag{8}$$

where $\varepsilon_{\mathrm{pa}}$ is true plastic strain amplitude, $\varepsilon_{\mathrm{ta}}$ is the total strain amplitude, σ_a the true stress amplitude, and E is the Young's modulus.

Fig. 10 shows the log-log plot for the number of reversals versus true stress amplitude obtained after converting the data as described. The equation shown is the resulting power law from the data which is equivalent to (4). Fig. 11 shows the log-log plot for number of reversals versus true plastic strain amplitude. The equation in the plot represents the power law that was given in (5). From the log-log plots, $\sigma'_f = 417.7$, $b = -0.0855$, $\varepsilon'_f = 0.0035$, and $c = -0.110$.

V. Discussion

Fatigue tests performed at $R = 0.5$ showed no I_c degradation for maximum strain of 0.350% and 0.367%. The *n-values* for these samples remain unchanged. Microscopy showed no cracks in these samples. With increasing N, however, a gradual degradation in I_c was observed in samples with maximum strains of 0.380% and 0.400%. This indicates that crack nucleation and growth (widening) were slow. This may also be due to the fact that the fatigue loads were applied in strain-controlled mode so fast crack formation and widening as observed in the microstructural images from such samples in Fig. 7 would not be expected.

Of the $R = 0.2$ samples, only that with 0.350% maximum strain showed no degradation. Sharp I_c degradation was observed for all other $R = 0.2$ samples with the fatigue lives decreasing as $\varepsilon_{\max}$ increased. The *n-value* for these samples also shows degradation with increasing N. The sharp I_c degradation for these samples is due to the fact that the maximum strains were higher than the $R = 0.5$ samples. Consequently, the crack formation and widening is faster and larger cracks are observed in the microstructural images [Fig. 8(a)].

Noting that all observed cracks initiate at the conductor edge, it appears that the slitting process damages the edges of the superconductor and that this damage serves as crack nucleation sites during fatigue. The cracks grow/widen with an increasing number of cycles if the applied strain is sufficiently high. Cheggour *et al.* [13] cautioned that though they did not observe I_c degradation in their loading case (transverse fatigue), a different loading case (in this case longitudinal fatigue) may show that the slitting process has detrimental effects on conductor electromechanical performance.

It is interesting to take a closer look at the $I_c(N)$ and $n(N)$ behavior in the high cycle fatigue regime. Figs. 12 and 13 show the data for $N > 10\,000$ for two cases: $R = 0.5$, maximum strain $= 0.380\%$ (Fig. 12) and $R = 0.2$, maximum strain $= 0.450\%$ (Fig. 13). In both cases, a reduction in I_c is observed. In Fig. 12, the *n-value* decreases in parallel with I_c at $N = 29\,400$. As N approaches 100 000 cycles, the *n-value* begins to oscillate and then decreases, with a decrease in I_c shortly thereafter, corresponding to the end of the *n-value* oscillations. In the case of Fig. 13, two spikes in *n-value* are observed, each corresponding to a subsequent decrease in I_c. Figs. 14 and 15

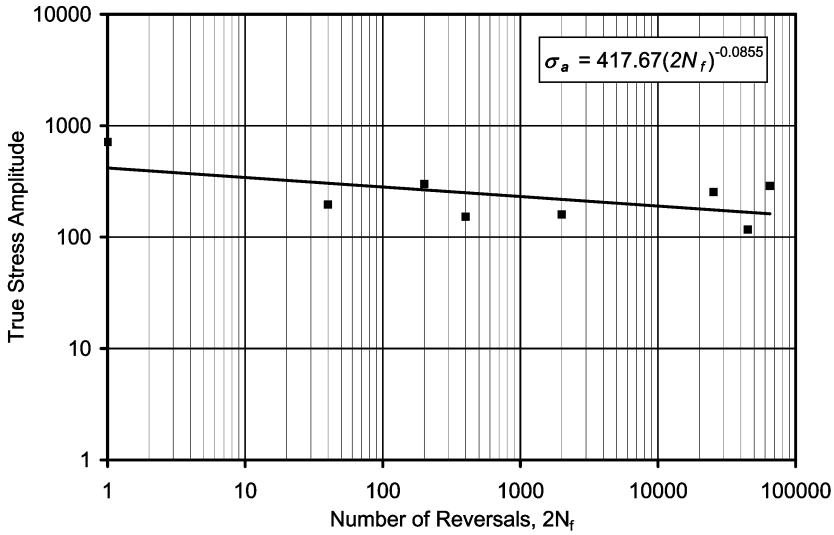

Fig. 10. Number of reversal versus true stress amplitude plot on a log-log scale for the data obtained during fatigue tests. The equation inset represents the power law [Equation (4)].

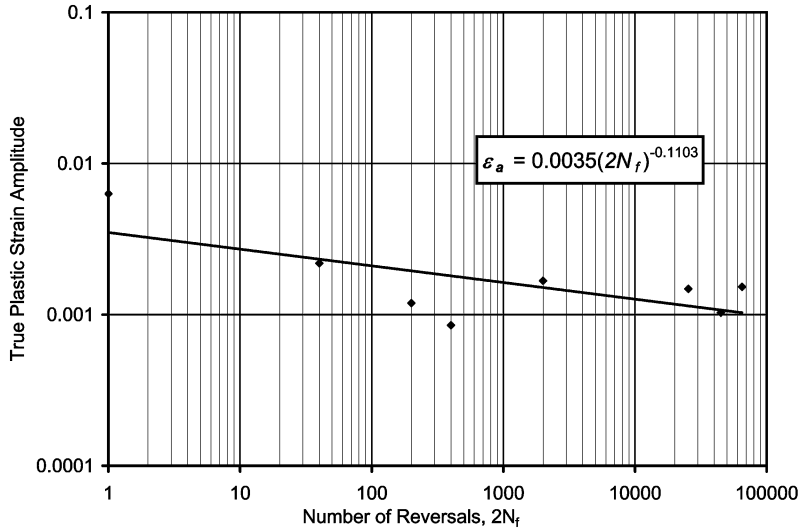

Fig. 11. Number of reversals versus true plastic strain amplitude plot on a log-log scale. The equation insert in the plot is the power law [Equation (5)].

show the same range of N-data for two cases where there is no degradation in I_c: $R = 0.5$, maximum strain $= 0.367\%$ (Fig. 14) and $R = 0.2$, maximum strain $= 0.350\%$ (Fig. 15). In these cases, the n-*value* begins to oscillate significantly for $N >\sim 50\,000$. For $R = 0.5$ (Fig. 14), the oscillations are about $\pm 15\%$, but there is no significant change in the average value. For $R = 0.2$, the magnitude of the oscillations is about the same, but there is a systematic increase in n-*value* of about 25%. In both cases, the I_c data is uniform. Considering that in both of these cases, the next highest increment of maximum strain resulted in reduced I_c, it is possible that the oscillations in n-*value* are a precursor and indicator of impending degradation in I_c. As N increases, the strain field around the tips of any existing cracks will also increase and can influence flux pinning and thus n-*value*. When the crack grows, the strain is released and, depending on the available current paths in the superconductor, I_c might also decrease. The correlation whereby the n-*value* oscillates or increases just prior to a decrease in I_c is not observed in every sample or with every decrease in I_c. This could easily be understood as being related to the insufficient resolution in the $I_c(N)$ and $n(N)$ data that results from the impracticality of making an I_c measurement after every cycle in high cycle fatigue, but it leaves the interpretation inconclusive. Performing the I_c measurements in a background magnetic field, where the effects of changes in flux pinning may be amplified, may give a better understanding of the correlation between n-*value*, I_c and N.

The fatigue strength coefficient σ_f' is approximately equal to the true fracture strength of the material [21]–[23]. The value of b varies between -0.04 and -0.15 for metals [24]. The fatigue strength coefficient determined from the fatigue data, $\sigma_f' = 417.7$ shows that the YBCO tapes would fail at a value of 417.7 MPa in fatigue. This is $\sim$56% of the yield stress of the conductor, (740 MPa) found on the single cycle test. The fatigue strength exponent, b from the data, is -0.0855, is within the range given in literature for metals (-0.04 to -0.15). This

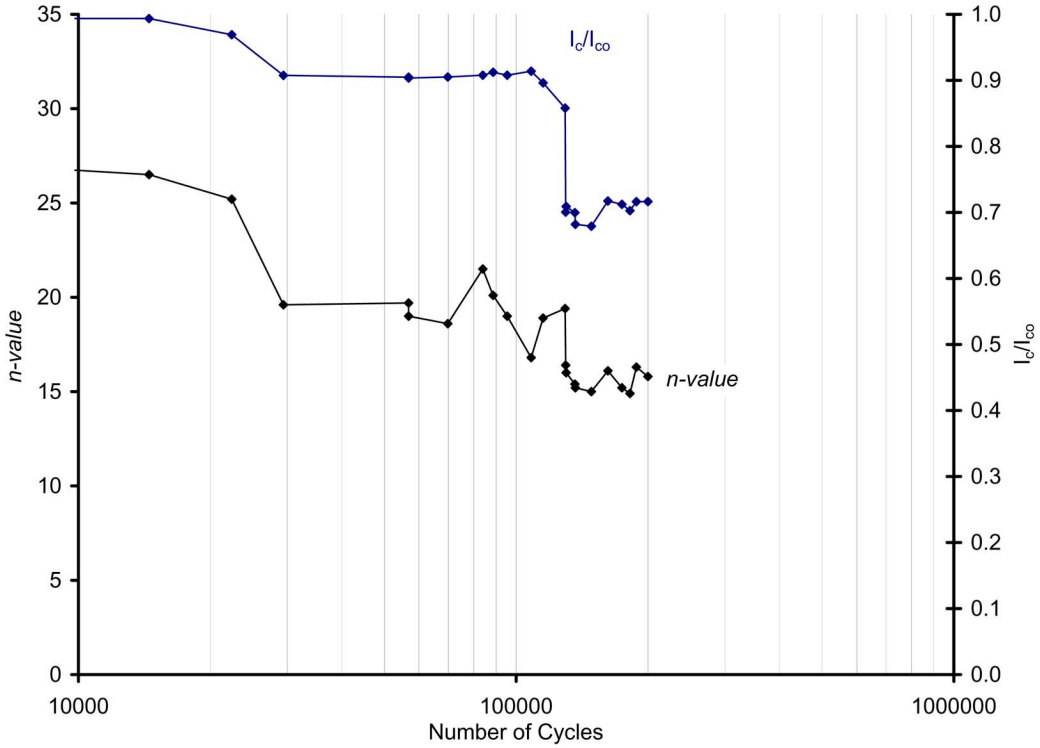

Fig. 12. *n-value* and normalized I_c versus N for a sample fatigued with $R = 0.5$ and $\varepsilon_{\max} = 0.380\%$. The *n-value* is at times decreasing with I_c for the same N and increases sharply before I_c degrades.

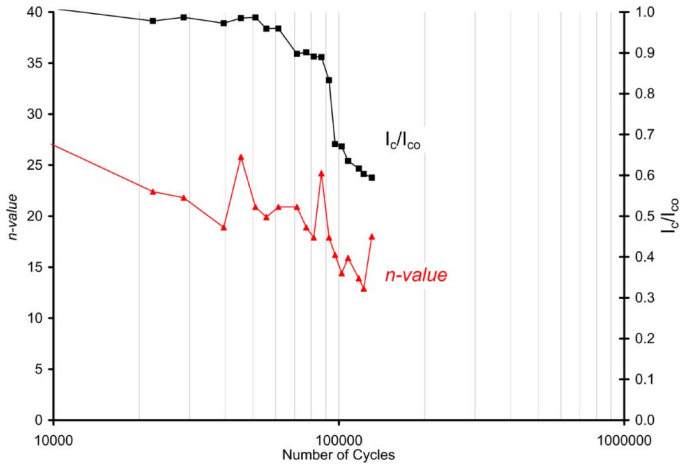

Fig. 13. *n-value* and normalized I_c versus N for a sample fatigued with $R = 0.2$ and $\varepsilon_{\max} = 0.450\%$. The *n-value* is at times decreasing or increasing with I_c for the same N and at times is oscillatory with N.

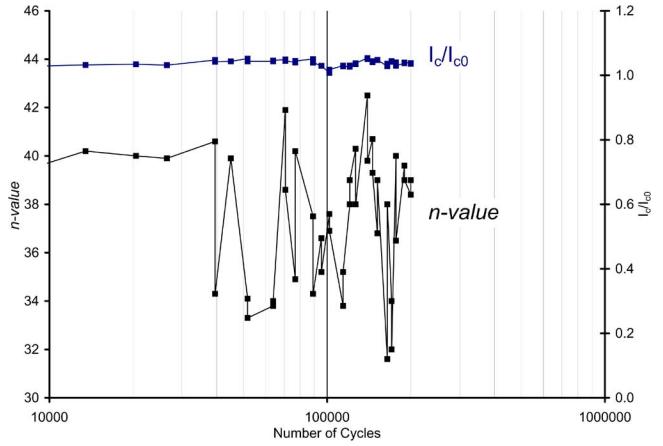

Fig. 14. *n-value* and normalized I_c versus N for a sample fatigued with $R = 0.5$ and $\varepsilon_{\max} = 0.367\%$. The *n-value* is at times decreasing or increasing with I_c for the same N and at times is oscillatory with N.

implies that the fatigue strength is primarily determined by the metal layers in the composite conductor.

The ductility coefficient ε'_f is approximately equal to the true fracture ductility coefficient for the material [21], [22]. For a fairly ductile material, where $\varepsilon'_f \sim 1$, the average value of c is -0.6, and for strong metals where $\varepsilon'_f = 0.5$, the average value of c is -0.5 [21]. The exponent c varies between -0.3 and -1.0 for metals [24]. The fatigue ductility coefficient obtained here is 0.0035 and the ductility exponent $c = -0.110$, which do not fall within the range given for metals and shows that this composite does not behave like a ductile material. Thus, though the major components of the superconducting tapes are metals, the ductility properties as determined by the 95% I_{co} criteria depends on the YBCO layer which is brittle, and not sample breaking as is done in fatigue tests for other materials.

VI. Conclusion

Crack formation is believed to be the cause of I_c degradation in fatigued samples. The cracks formed during fatigue tests do not occur everywhere in the sample but are localized in areas which are weak or where defects are introduced by the slitting

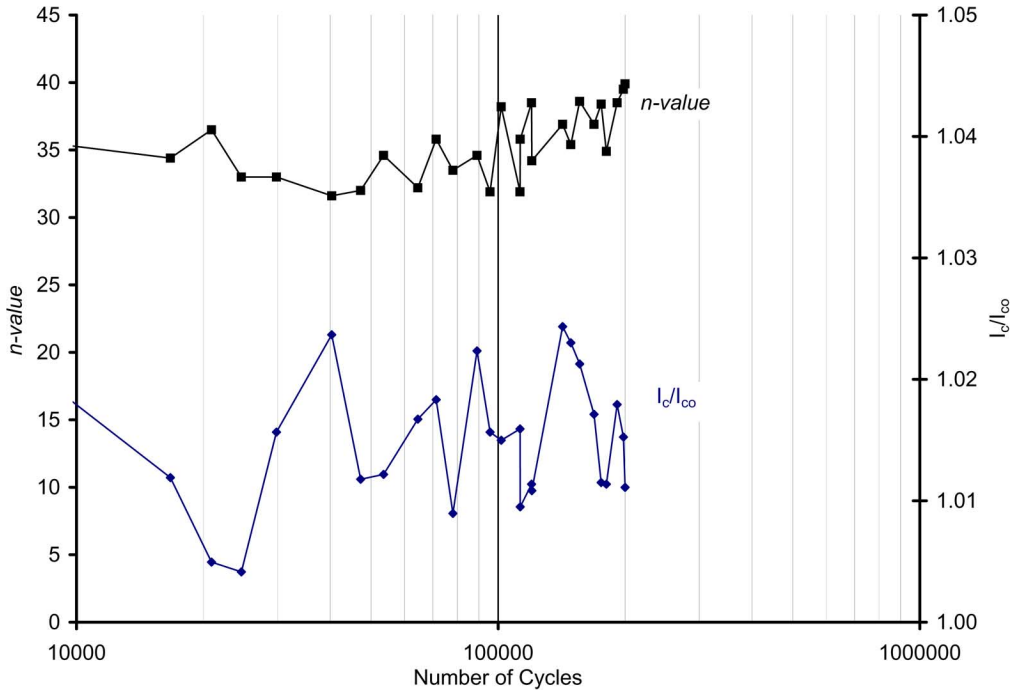

Fig. 15. Normalized n-*value* and I_c versus N for a sample fatigued with $R = 0.2$ and $\varepsilon_{\max} = 0.350\%$. The n-*value* is at times decreasing or increasing with I_c for the same N and at times it is oscillatory with N.

process. Cracks initiate at the sample edges and propagate (meander) towards the sample center. Further, the size and quantity of the cracks is related to the I_c degradation.

I_c degraded at a faster rate for all samples with $R = 0.2$ than for those with $R = 0.5$, implying faster crack growth which may be due to the higher strain limit and thus higher strain range in the $R = 0.2$ case. I_c did not degrade for tests performed with a maximum strain of 0.350% for both $R = 0.2$ and $R = 0.5$ up to $N = 2 \times 10^5$. Also, for $R = 0.5$ a limit has been observed for 0.367% maximum strain.

The fatigue strength and ductility behaviors were analyzed using a 5% reduction in I_c as the electrical definition of failure. The fatigue strength exponent is within the values found for metals but both the fatigue ductility coefficient and exponent show that the material tested is brittle. Thus, the electromechanical fatigue behavior is interpreted as being influenced by a combination of the ductile metal substrate and the brittle ceramic transport carrier layer (superconductor). Note that if a different definition of failure is used (resulting in a different criterion for determining the number of reversals), these values may change. For example, for a 10% I_c degradation as definition of failure, the number of cycles should be read when the I_c crosses 90% I_{c0} for each sample. New plots for true stress amplitude and true plastic strain amplitude versus number of reversals (with new number of reversals) would result in new coefficients and exponents.

ACKNOWLEDGMENT

The authors would like to thank SuperPower Inc. for providing the YBCO coated conductor that was used in this work.

REFERENCES

[1] P. J. Masson, G. V. Brown, D. S. Soban, and C. A. Luongo, "HTS machines as enabling technology for all-electric airborne vehicles," *Supercond. Sci. Technol.*, vol. 20, pp. 748–756, 2007.

[2] H. Kitaguchi, K. Itoh, H. Kumakura, T. Takeuchi, K. Togano, and H. Wada, "Strain and fatigue tests on Bi-2223/Ag superconducting tapes," *Physica C*, vol. 357–360, pp. 1193–1196, 2001.

[3] M. Sugano, K. Osamura, and S. Ochiai, "Change of critical current of Ag/Bi2223 tapes under fatigue test," *Adv. Cryog. Eng., Materials*, vol. 48, pp. 485–491, 2002.

[4] M. T. Malachevsky and D. A. Esparza, "Metal-ceramic interface response to bending and fatigue cycles in superconducting Ag-Bi2223 composites," *Physica C*, vol. 324, pp. 153–160, 1999.

[5] R. L. Holtz and D. U. Gubser, "High cycle fatigue in high temperature superconductor motor applications," *J. Mater. Proc. Technol.*, vol. 117, no. 3, 2001.

[6] R. L. Holtz, S. Fleshler, and D. U. Gubser, "Fatigue of a reinforced high temperature superconducting tape," *J. Adv. Eng. Mater.*, vol. 3, no. 3, pp. 131–134, 2001.

[7] A. Salazar, J. Y. Pastor, and J. LLorca, "Fatigue behavior of multifilamentary BSCCO 2223/Ag superconducting tapes," *IEEE Trans. Appl. Supercond.*, vol. 14, no. 3, pp. 1941–1947, Sep. 2004.

[8] H. Shin, J. R. C. Dizon, K. Kim, S. Oh, and D. Ha, "Mechanical and transport properties of Ag alloy/Bi-2223 superconducting tapes under axial fatigue loading," *Physica C*, vol. 436–431, pp. 1188–1193, 2005.

[9] H. Shin, J. R. C. Dizon, K. Kim, S. Oh, and D. Ha, "I_c degradation behavior of Bi-2223 superconducting tapes under axial fatigue loading," *Cryogenics*, vol. 46, pp. 378–384, 2006.

[10] H. Shin, J. R. C. Dizon, K. Kim, S. Oh, and D. Ha, "Fatigue behavior and its influence on the critical current of externally reinforced Bi-2223 superconducting tape," *IEEE Trans. Appl. Supercond.*, vol. 15, no. 2, pp. 3556–3559, Jun. 2005.

[11] J. W. Ekin, S. L. Bray, N. Cheggour, C. C. Clickner, S. R. Foltyn, P. N. Arendt, A. A. Polyanskii, D. C. Larbalestier, and C. N. McCowan, "Transverse stress and fatigue effects on Y–Ba–Cu–O coated Ibad tapes," *IEEE Trans. Appl. Supercond.*, vol. 11, no. 1, pt. 3, pp. 3389–3392, Mar. 2001.

[12] N. Cheggour, J. W. Ekin, C. C. Clickner, R. Feenstra, A. Goyal, M. Paranthaman, D. F. Lee, D. M. Kroeger, and D. K. Christen, "Transverse compressive stress, fatigue, and magnetic substrate effects on the critical current density of Y–Ba–Cu–O coated RABiTS tapes," *Adv. Cryo. Eng.*, vol. 48, pp. 461–468, 2002.
[13] N. Cheggour, J. W. Ekin, C. L. H. Thieme, and Y. Xie, "Effects of fatigue under transverse compressive stress on slit Y–Ba–Cu–O coated conductor," *IEEE Trans. Appl. Supercond.*, vol. 17, no. 2, pp. 3063–3066, Jun. 2007.
[14] IGC SuperPower Press Release, SuperPower Continues to Set the Pace of Global Leadership in Second Generation High-Temperature Wire Jul. 25, 2006.
[15] A. L. Mbaruku, U. P. Trociewitz, and J. Schwartz, "Development of a low-temperature electro-mechanical testing device," *IEEE Trans. Appl. Supercond.*, vol. 15, no. 2, pt. 3, pp. 3620–3623, Jun. 2005.
[16] A. L. Mbaruku, *Electromechanical and Fatigue Properties of As-Manufactured and Quench Damaged YBCO Coated Conductor*. Tallahassee, FL: Department of Mechanical Engineering, Florida State University, 2006, pp. 39–65.
[17] J. Schwartz and H. W. Weijers, "Electrical measurements on superconductors by transport," in *Methods in Materials Research*, E. N. Kaufmann, Ed. *et al.* New York: Wiley, 2000, pp. 5b.5.1–5b.5.20.
[18] O. H. Basquin, "The exponential law of endurance tests," *Amer. Soc. Test. Mater. Proc.*, vol. 10, pp. 625–630, 1910.
[19] L. F. Coffin, "A study of the effects of cyclic thermal stresses on a ductile metal," *Trans. ASME*, vol. 76, pp. 931–950, 1954.
[20] S. S. Manson, "Behavior of materials under conditions of thermal stresses," in *Heat Transfer Symp.*, 1953, pp. 9–75.
[21] J. A. Bannantire, J. J. Comer, and J. L. Handrock, *Fundamentals of Metal Fatigue Analysis*. Englewood Cliffs, NJ: Prentice-Hall, 1990.
[22] B. Farahmand, G. Bockrath, and J. Glassco, *Fatigue and Fracture Mechanics of High Risk Parts: Applications of LEFM &FMDM Theory*. New York: Chapman & Hall, 1997.
[23] J. M. Barsom and S. T. Rolfe, *Fracture and Fatigue Control in Structures: Applications of Fracture Mechanics*. Englewood Cliffs, NJ: Prentice-Hall, 1987.
[24] Y. Lee, J. Pan, R. Hathaway, and M. Barkey, *Fatigue Testing and Analysis-Theory and Practice*. Burlington: Mass Elsevier, 2005.

Abdallah L. Mbaruku was born in Tanga, a city on the northeastern coast of Tanzania. He received the B.Sc. degree in mechanical engineering in 1991 from the University of Dar es Salaam-Tanzania and the Masters degree in mechatronics engineering from the University of Lancaster, U.K., in 1994. He also received the Ph.D. degree in mechanical engineering from Florida State University in 2006.

Between 1991 and 1993 he has worked as a Junior Development Engineer at the Institute of Production Innovation (IPI) of the University of Dar es Salaam. He has been working as an Assistant Development Engineer from 1994 to 2000 at IPI. His work involved research and development of appropriate technologies and teaching in the Department of Mechanical Engineering at the University of Dar es Salaam. From 2001, he worked with Professor Justin Schwartz in the field of high-temperature superconductors (HTS). His research focused on quench damage effects on electromechanical and fatigue properties of YBCO coated conductors. He has also worked on electromechanical characterization of AgMg Sheathed Bi-2212 tapes. He is currently with the Department of Engineering Materials of the College of Engineering and Technology, University of Dar es Salaam, Tanzania.

Justin Schwartz (M'91–SM'01–F'04) received the B.S. degree with Highest Honors in Nuclear Engineering in May 1985, and the Ph.D. degree in Nuclear Engineering from Massachusetts Institute of Technology, in 1990, where his Ph.D. thesis focused on the design of very high field toroidal field coils for fusion reactors.

He then spent six months as a Visiting Scientist at the National Research Institute for Metals, Japan, where he researched the processing and electromechanical properties of Bi–Sr–Ca–Cu–O high-temperature superconductor. In the fall of 1990, he joined the faculty of the Department of Nuclear Engineering at the University of Illinois Urbana as an Assistant Professor, and in 1993 he moved to the Department of Mechanical Engineering at the FAMU-FSU College of Engineering as an Associate Professor, and simultaneously as a group leader in the new National High Magnetic Field Laboratory of Florida State University (FSU). Since then, he has remained at FSU, where he is currently the Jack E. Crow Professor of Engineering. He leads research programs in the processing, properties, and application of high-temperature superconductors.